Chapter 2
Lens Correction and Gamma Correction

Sang-Bock Cho

Abstract Recently, the necessity of camera in vehicle industry is increasing now as increasing the smart car needs. Almost smart car concepts are implemented by using the camera system based on image processing technology. Actually, the rear view camera for parking assistance system, the forward view camera for lane departure warning and forward collision warning system, and multi-view camera for vehicle black box and blind spot warning system and so on, so many systems those adopted the camera system are already released. However, performance of these functions strongly depends on the image quality through the camera system. Especially, distortion of a thing pictured by the lens and suddenly illumination changing by environments are core factors affecting the image quality for smart car performance. Thus, in this chapter, we introduced a vehicle friendly lens correction algorithm and a gamma correction algorithm with objective illumination estimation method. In the lens correction part, we introduced a simple lens correction method in low-cost camera and we propose a method that leads to guarantee of the restrictions simultaneously for the determination. In the gamma correction part, we introduced the objective illumination estimation methods and the gamma correction methods based on tone mapping.

2.1 Lens Correction

2.1.1 Introduction to Lens Correction

Cameras being used in the field have been having lens distortion, and it has been considerably dealing in image process area. So far, many lens correction algorithms have been relying on the invariant properties of projective geometry in

S.-B. Cho (✉)
School of Electrical Engineering, University of Ulsan, Ulsan, Korea
e-mail: sbcho@ulsan.ac.kr

J. Kim and H. Shin (eds.), *Algorithm & SoC Design for Automotive Vision Systems*, DOI: 10.1007/978-94-017-9075-8_2,

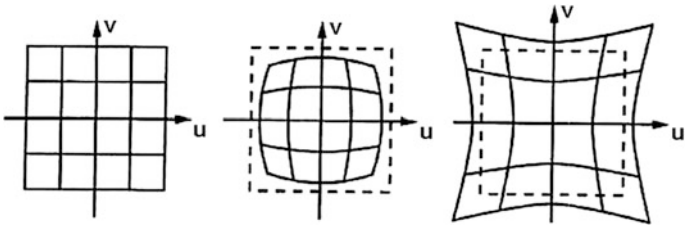

Fig. 2.1 Radial distortions—ideal image with no distortion, barrel distortion, and pincushion distortion (*from left to right*)

order to find distortion parameters. A common property is "the straight line in scene is straight line in image". However, if the straight lines are also parallel together, the previous works have missed this restriction in determining lens distortion parameters.

Model of lens distortion was proposed by Brown [1, 2] including radial distortion, decentering distortion and prism distortion. Radial distortion (barrel distortion or/and pincushion distortion) as shown in Fig. 2.1 is noticeable but other distortions are acceptably negligible.

Many algorithms adopted this model used 3D reference points to find the lens distortion parameters [3–9]. However, these algorithms can find the proper distortion parameter only when their experiments were precise and extracting control points were accurate.

In another class of lens distortion correction, there have been many proposed methods based on geometric invariants of some features to achieve distortion parameters [10–14]. The straight property of line—the straight line in scene is straight line in image—is used widely. However, if the straight lines are also parallel together, these methods have missed this restriction in determining lens distortion parameters. This can cause wrong distortion parameters of final solution in search algorithm. Finally, the other approaches were proposed to correct lens distortion that collect whole content of image to get distortion parameters [15–17]. These approaches take advantage of image content without requiring any pattern calibration. However, results are still limited to lead to convincing results.

Model of lens distortion was proposed by Brown [1, 2] including radial distortion, decentering distortion and prism distortion. Radial distortion (barrel distortion or/and pincushion distortion) is noticeable and other distortions are acceptably negligible, as shown in Fig. 2.1. The adopted methods to this model [3–8, 14] used 3D reference points to find lens distortion parameters. These methods encountered in setting up experiments precisely and extracting control points accurately under noise impact. In another class of lens distortion correction, there have been many proposed methods based on geometric invariants of some features to achieve distortion parameters [7, 10, 12, 18]. The straight property of line—the straight line in scene is straight line in image—is used widely. However, if the straight lines are also parallel together, these methods have missed this restriction in determining lens distortion parameters. Finally, the other approaches

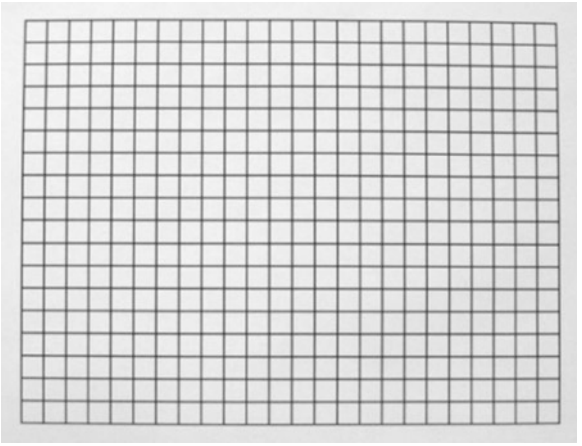

Fig. 2.2 Standard calibration template

were proposed to correct lens distortion that collect whole content of image to get distortion parameters [8, 15, 18]. These approaches take advantage of image content without requiring any pattern calibration. However, results are still limited to lead to convincing results.

In this chapter, our proposed method is based on the projective transformation "a straight line in a 3D scene domain is itself straight line in the 2D image domain" [2]. This means that curvature of lines in the image that should be straight is due only to lens distortion. Using this principal, iterative search algorithms are applied to seek adequate distortion parameters, which make cure lines in image become its original state—the straight lines. The proposed method in this chapter is different from above works. We use a template consisting of lines that are straight, parallel and perpendicular together, as shown in Fig. 2.2. After the correction, the restrictions of lines of template are guaranteed.

2.1.2 Lens Distortion Model

The standard model for the radial and decentering distortion is mapping from the distorted image coordinates $q_d = (u_d, v_d)$ that are observable to the undistorted image coordinates $q_p = (u_p, v_p)$ which are not physically measurable.

$$u_p = u_d + \overline{u_d}\left(k_1 r_d^2 + k_2 r_d^4 + k_3 r_d^6 + \cdots\right) + \left[p_1\left(r_d^2 + 2\overline{u_d^2}\right) + 2p_2\overline{u_d v_d}\right]\left[1 + p_3 r_d^2 + \cdots\right] \tag{2.1a}$$

$$v_p = v_d + \overline{v_d}\left(k_1 r_d^2 + k_2 r_d^4 + k_3 r_d^6 + \cdots\right) + \left[p_1\left(r_d^2 + 2\overline{v_d^2}\right) + 2p_2\overline{u_d}\,\overline{v_d}\right]\left[1 + p_3 r_d^2 + \cdots\right] \tag{2.1b}$$

where

$$\overline{u_d} = u_d - c_u, \quad \overline{v_d} = u_d - c_v, \quad r_d^2 = \overline{u_d^2} + \overline{v_d^2} \tag{2.1c}$$

and k_1, k_2, k_3,… are coefficients of radial distortion and p_1, p_2, p_3,… are coefficients of decentering distortion, r_d is the radius of an image point from the distortion center defined as (c_u, c_v) above.

Typically, since we only consider two coefficients of radial distortion [5, 7, 12, 18] the model after discarding other terms:

$$u_p = u_d + \overline{u_d}\left(k_1 r_d^2 + k_2 r_d^4\right) \tag{2.2a}$$

$$v_p = v_d + \overline{v_d}\left(k_1 r_d^2 + k_2 r_d^4\right) \tag{2.2b}$$

$$r_p = r_d\left(1 + k_1 r_d^2 + k_2 r_d^4\right) \tag{2.2c}$$

Therefore, the lens distortion correction becomes recovering the practically significant distortion coefficients k_1, k_2 and distortion center (c_u, c_v).

2.1.3 Proposed Method

2.1.3.1 Basic Idea

The standard calibration template as shown in Fig. 2.2, it consists of black straight lines in horizontal and vertical directions. These lines are parallel and perpendicular together on bright background. In horizontal direction, on a horizontal line that is the nearest to distortion center, we find out the intersection points of this horizontal line with vertical lines. Based on each intersection point, we count the number of pixels of vertical line which cross the intersection point. Since lens distortion exists, the number of pixels of the vertical line do not lie on vertical axis (origin of vertical axis is intersection point). We measure the farthest distance of pixels of each line to vertical axis respectively at each base point and seek lens distortion parameters of camera by minimizing this distance. The process is the same for vertical direction. Figure 2.3 shows the position of pixels in horizontal direction of a non-distorted image and a distorted image.

First of all, a binary image is made of a gray image. In the binary image, there are horizontal lines and vertical lines; the width of these lines is one pixel. Then the distortion center is initialized, e.g. image center. In horizontal direction, since a straight line crossing the distortion center is still straight line in distorted image, so a horizontal line that is through the distortion center (or the nearest the distortion center) is chosen. This line is named as driven line.

On the driven line, the points where vertical lines intersect with this line can be determined. These points are named base points. The number of the base points is

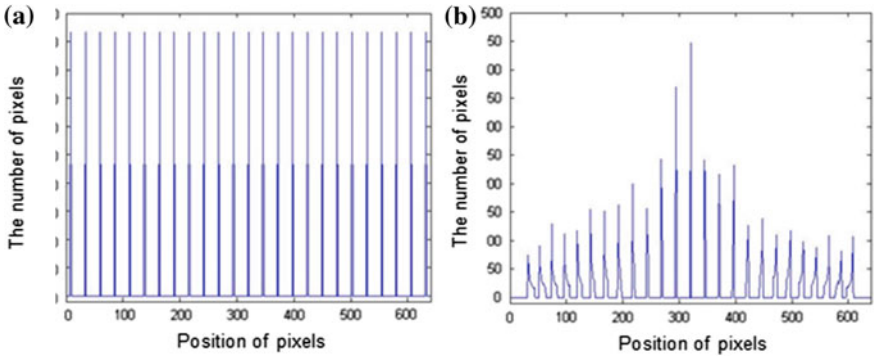

Fig. 2.3 The number of pixels in horizontal direction, **a** in non-distortion image, **b** in distortion image

equal the number of vertical lines n. Based on each base point, in next step, we count the number of pixels of respective vertical line. Due to lens distortion, a number of pixels of vertical line do not lie on vertical axis (the origin of vertical axis is base point). In the close range of each base point, we determine one point on the left and another one on the right of base point where the number of pixels at these two points are greater than e pixels (in our implementation, $e = 4$). They are called up-position points and down-position points. Therefore, each base point lies on the range between up-position point and down-position point respectively. We evaluate the distortion by measuring the distances from up-position points p_i^{uh} to down-position points p_i^{dh} respectively. This measurement is defined by a function E_1 as

$$E_1 = \sum_{i=1}^{n} \sqrt{\left(p_i^{uh} - p_i^{dh}\right)^2} \Big/ n \tag{2.3}$$

The process is the same as in vertical direction. We have:

$$E_2 = \sum_{i=1}^{m} \sqrt{\left(p_i^{uv} - p_i^{dv}\right)^2} \Big/ m \tag{2.4}$$

Finally, we define a function E as evaluation of distortion in whole image:

$$E = (E_1 + E_2)/2 \tag{2.5}$$

where n and m are the number of vertical lines and horizontal lines, p_i^{uh} and p_i^{uv} are the up-position points in horizontal and vertical direction, and p_i^{dh} and p_i^{dv} are the down-position points in horizontal and vertical direction.

The error E reflects the farthest distance of pixels of each line to axis respectively at each base point. Minimization of the error function E is our goal for

seeking distortion parameters. In this chapter, we optimize distortion parameters using the Nelder-Mead simplex method [9].

2.1.3.2 Linear Form Solution

Nonlinear optimization algorithm is an iterative progress and initial value plays an important role to lead to an exactly converged value. If initial value is so far from global minima, converged value can be a local minima and results in a false solution. In this chapter, we adopted the method in [5] for initial guess. The method is summarized as follows:

Suppose we have a line l in the undistorted image plane. Every point (u_p, v_p) on the line satisfies the equation

$$au_p + bv_p + c = 0 \tag{2.6}$$

where a, b and c are constants for specific line l, with—a/b being the line slope. Each point on the line is related to a point (u_d, v_d) in the distorted image plane according to Eq. (2.1). This means that both coordinate of the line point are functions of (u_d, v_d). Therefore, the last equation can be written as

$$f(u_d, v_d) = au_p(u_d, v_d) + bv_p(u_d, v_d) + c = 0 \tag{2.7}$$

where $f(u_d, v_d)$ describes the equation of the corresponding cure in the distorted image plane. The elemental change in f at any distorted image point (u_d, v_d) can be expressed as

$$\delta f = a\left[\frac{\partial u_p}{\partial u_d}\delta u_d + \frac{\partial u_p}{\partial v_d}\delta v_d\right] + b\left[\frac{\partial v_p}{\partial u_d}\delta u_d + \frac{\partial v_p}{\partial v_d}\delta v_d\right] = 0 \tag{2.8}$$

where all the four partial derivatives can be directly computed from Eq. (2.1). Hence, one can see that the slope of the line S in the undistorted plane (which should equal—a/b) is related to the slope of the tangent $(\delta v_d/\delta u_d)$ to the curve at point (u_d, v_d) by

$$s(u_d, v_d) = \left(\frac{\partial v_p}{\partial u_d} + \frac{\partial v_p}{\partial v_d}\frac{\partial v_d}{\partial u_d}\right) \Big/ \left(\frac{\partial u_p}{\partial u_d} + \frac{\partial u_p}{\partial v_d}\frac{\partial v_d}{\partial u_d}\right) \tag{2.9}$$

In our case, we choose some lines in image template as reference lines in finding linear solution. We only estimate k_1 and k_2 equation of linear form solution $Ax = b$ can expressed as

$$A = \begin{bmatrix} a_{11} & a_{12} \\ a_{21} & a_{22} \end{bmatrix},\ x = \begin{bmatrix} k_1 \\ k_2 \end{bmatrix} \text{ and } b = \begin{bmatrix} \hat{s}_1 - s_{1,1} \\ \hat{s}_2 - s_{2,1} \end{bmatrix} \tag{2.10a}$$

with

$$\begin{aligned} a_{11} &= 2\bar{u}_{1,1}\bar{v}_{1,1}\left(1-\hat{s}_1 s_{1,1}\right)+\left(\bar{u}_{1,1}^2+\bar{v}_{1,1}^2\right)\left(s_{1,1}-\hat{s}_1\right) \\ &\quad +2\left(\bar{v}_{1,1}^2 s_{1,1}-\bar{u}_{1,1}^2\hat{s}_1\right) \end{aligned} \tag{2.10b}$$

$$\begin{aligned} a_{12} &= 4\bar{u}_{1,1}\bar{v}_{1,1}\left(\bar{u}_{1,1}^2+\bar{v}_{1,1}^2\right)\left(1-\hat{s}_1 s_{1,1}\right)+\left(\bar{u}_{1,1}^2+\bar{v}_{1,1}^2\right)\left(s_{1,1}-\hat{s}_1\right) \\ &\quad +\left(\bar{u}_{1,1}^2+\bar{v}_{1,1}^2\right)\left(\bar{v}_{1,1}^2 s_{1,1}-\bar{u}_{1,1}^2\hat{s}_1\right) \end{aligned} \tag{2.10c}$$

$$\begin{aligned} a_{21} &= 2\bar{u}_{2,1}\bar{v}_{2,1}\left(1-\hat{s}_2 s_{2,1}\right)+\left(\bar{u}_{2,1}^2+v_{2,1}^2\right)\left(s_{2,1}-\hat{s}_2\right) \\ &\quad +2\left(\bar{v}_{2,1}^2 s_{2,1}-\bar{u}_{2,1}^2\hat{s}_2\right) \end{aligned} \tag{2.10d}$$

$$\begin{aligned} a_{22} &= 4\bar{u}_{2,1}\bar{v}_{2,1}\left(\bar{u}_{2,1}^2+\bar{v}_{2,1}^2\right)\left(1-\hat{s}_2 s_{2,1}\right)+\left(\bar{u}_{2,1}^2+\bar{v}_{2,1}^2\right)\left(s_{2,1}-\hat{s}_1\right) \\ &\quad +\left(\bar{u}_{2,1}^2+\bar{v}_{2,1}^2\right)\left(\bar{v}_{2,1}^2 s_{2,1}-\bar{u}_{2,1}^2\hat{s}_1\right) \end{aligned} \tag{2.10e}$$

where $\left(u_{l,i}, v_{l,i}\right)$ denotes the i-th distorted point on chain l with tangent slope $s_{l,i}, \hat{s}_l$ is the estimated slope of the line corresponding to chain l. The slope $s_{l,i}$ is estimated by approximating the curve points within a window of size 2W + 1 (in our implementation, W = 5) by a second order polynomial.

2.1.3.3 Straight Line Method

Given a set of distorted points (u_d, v_d) in the lines of distorted image, in search algorithms, a set of the distortion parameters is applied to the distorted points. Lines are fitted to the resulting points (corrected points) $\left(u_p, v_p\right)$ and objective function is computed as the sum of the squared distances of the corrected points from their corresponding best-fit straight lines.

Let the best-fit straight line for a set of corrected points be:

$$u_p \sin\theta - v_p \cos\theta + \rho = 0 \tag{2.11}$$

where θ is the angle the line makes with the horizontal axis and ρ is the distance of the line from the distortion center. Therefore, the error due to a single point is given by:

$$e = \left(u_p \sin\theta - v_p \cos\theta + \rho\right)^2 \tag{2.12}$$

where the values for $\left(u_p, v_p\right)$ are calculated from the correction equation Eq. (2.1). Let the number of the lines in the distorted image is L, and let the number of points on each line l be t_l. Then, the objective junction is given by:

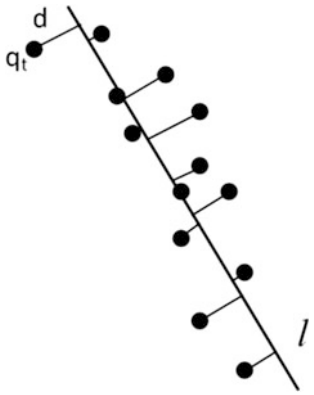

Fig. 2.4 Best-fit straight line of a set of points

$$\xi = \sum_{l=1}^{L} \sum_{p=1}^{t_l} \left(u_p^{t,l} \sin\theta_l - v_p^{t,l} \cos\theta_l + \rho_l \right)^2 \tag{2.13}$$

where θ_l and ρ_l are the best-fit straight line parameters corresponding to the line l and $\left(u_p^{t,l}, v_p^{t,l}\right)$ is the corrected point to the line l. After getting the objective function, the distortion parameters are found out by minimizing this function using some non-linear search algorithms (Fig. 2.4).

2.1.4 Experimental Result

To evaluate performance of the proposed method, we carry out experiments on synthetic images and real images. In simulation, the distorted-synthetic images are created by warping the undistorted-synthetic template images with radial distortion model expressed in Eq. (2.11)

$$r_p = r_d \left(1 + k_1 r_d^2 + k_2 r_d^4\right) \tag{2.14}$$

While distortion coefficient k_2 is fixed due to the weak impact compared with k_1, distortion coefficient k_1 is changed for testing. In our experiment, $k_2 = 3 \times 10^{-13}$, $k_1 = -8 \times 10^{-7} : -4.8 \times 10^{-7}$. Then, we recover the undistorted images from these distorted images using the linear solution, the straight line method and the proposed method. After completing the lens distortion correction, the performances of each method are evaluated based on the error in Eq. (2.5).

The errors of each method are shown in Fig. 2.5. In the first view, we see that the error of the linear method is the worst among three methods. The result also shows that distortion correction based on straight line method causes the error greater than the proposed method when it just guarantees straight restriction of

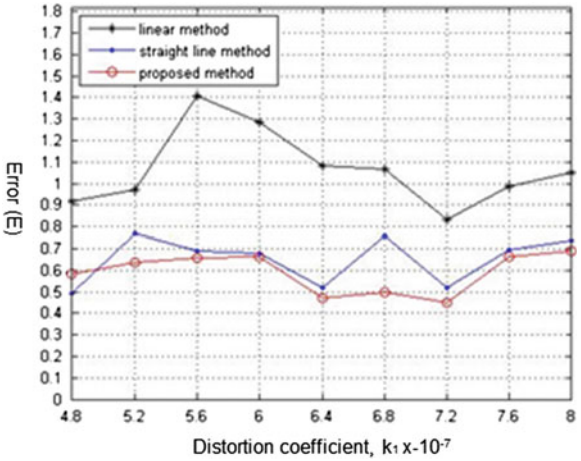

Fig. 2.5 Error of the methods after correcting distortion

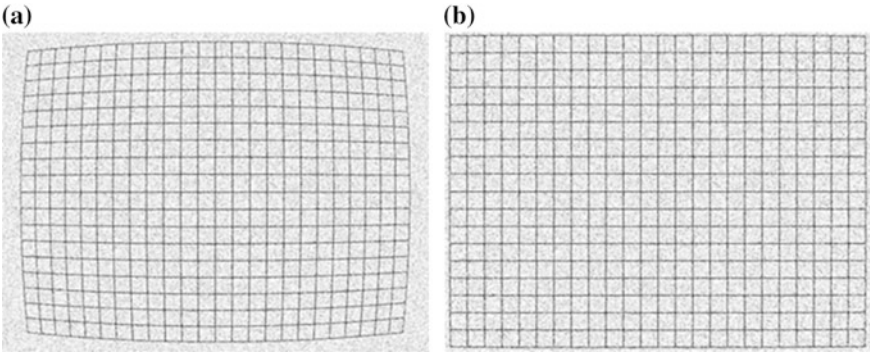

Fig. 2.6 The impact of noise in the proposed method (**a** input image, lens distorted image via camera, **b** lens distortion corrected image). Lens distorted image via camera (**a**), lens distortion corrected image (**b**)

each line without guaranteeing the parallel restriction among straight lines. By applying our method, however, these restrictions are guaranteed more stringent in distortion correction because they are considered simultaneously. It means that almost vertical lines (horizontal lines) coincide with vertical axes (horizontal axes) respectively at each base point.

In Fig. 2.6, we consider the noise impact in our method. The distorted-synthetic images are corrupted by zero-mean Gaussian noise of standard deviation 0.2 pixels. From the experiment, although the noise impact causes our image content to be very erroneous from original image content, corrected image is almost the same ideal image that is taken from pinhole camera model. Therefore, under the influence of noise in practical cases, the proposed method is better than other methods to correct lens distortion.

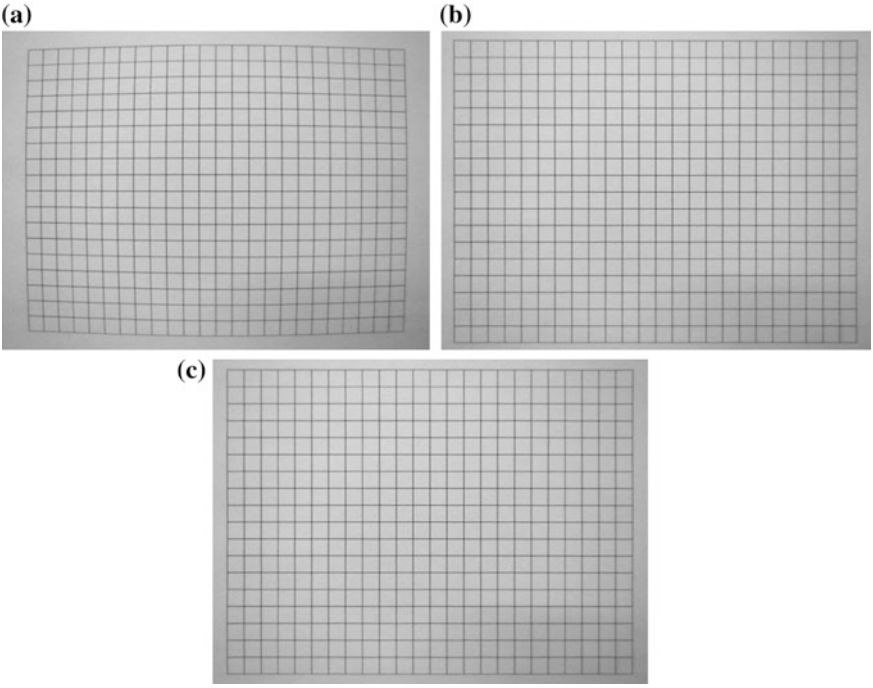

Fig. 2.7 Radial distortion correction of three methods: **a** distorted image, **b** straight line method, **c** lens distortion corrected image by using the proposed method

2.1.5 Conclusion

To evaluate the effectiveness of the proposed method in practical case, Fig. 2.7 shows the radial distortion correction of camera Canon SX20IS using the straight line method and the proposed method. The error before correcting is 4.0758; and after correcting is 0.6821, 0.6421 of the straight line method, and our method respectively.

Figure 2.8 shows the result of radial distortion correction images by using the proposed method. In this chapter, a new method is presented for the lens distortion correction. Using a simple template including the parallel–perpendicular-straight lines, the method applies a common property of perspective geometry to seek the lens distortion parameters. This invariant property is expressed as "a straight line in a 3D scene domain is itself straight line in the 2D image domain". The previous works have used this property to find the lens distortion parameters when they try to straighten each line in the image that should be straight if there is no lens distortion. However, the method of this chapter is different from previous works. It determines the lens distortion parameters by minimizing the farthest distances of pixels on vertical lines (horizontal lines) to vertical axes (horizontal axes) respectively.

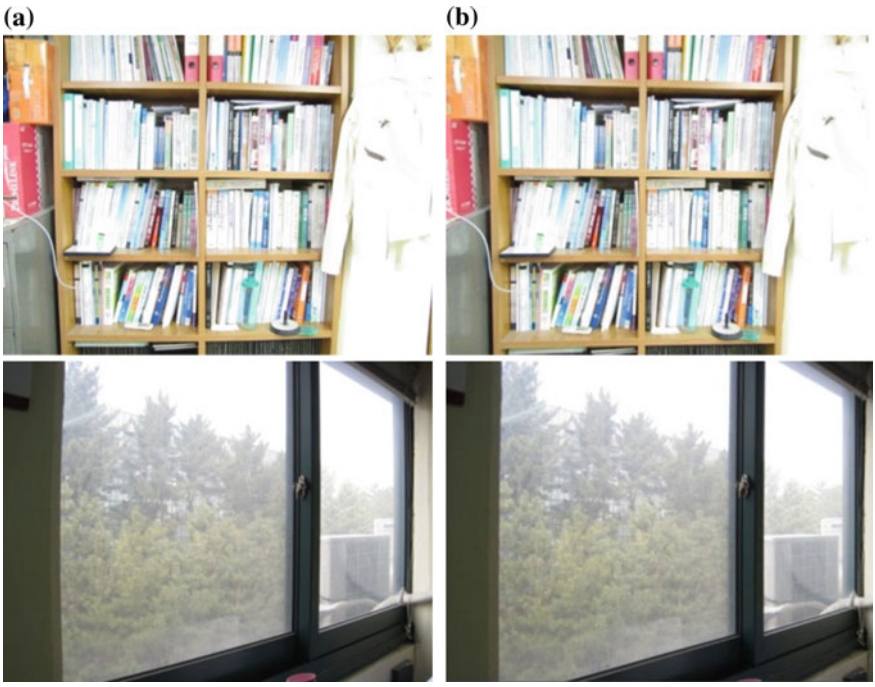

Fig. 2.8 Radial distortion correction results: **a** original distorted images, **b** corrected images

With the proposed method, it guarantees not only the straight property of each line but also the parallel property among lines for determining the distortion parameters. The experimental results prove the effectiveness and accuracy of the proposed method. Compared with the previous works, the error of the proposed method is almost less than that of the common methods when the distortion coefficient is changed from small value to large value. Moreover, the proposed method becomes more reliable and practical as it is verified under the impact of noise. In the experiment, the algorithm recovers the corrected image perfectly although the affect of noise on distorted image is serious.

In addition, this method is also provided the closed form solution in order to speed up the convergence and obviate the local minimum of objective function. Because the algorithm of the proposed method find out global minimum, the corrected image based on the distortion parameters will be close the ideal image taken from pinhole camera model.

In the future, the algorithm will be continued developing for more optimized process. First of all for improving purpose, we will get threshold automatically in converting from grayscale image to binary image. Next one is designing an adaptive coefficient(s) to reflect contribution of the distance from the distortion center in evaluating the distances between up positions and down positions respectively.

2.2 Gamma Correction

2.2.1 Normalized Numerical Image Descriptor

2.2.1.1 Introduction

The acquired image during the vehicle driving gets degraded by the ambient luminance condition and this is one of the big problems which need proper solution. Therefore, recently, the studies for the image quality enhancement by using the gamma correction method, wide dynamic range, etc., are activated. Almost numerous these studies have been based on the image quality assessment.

The assessment of image quality has been previously considered by Oakley and Bu [19]. One of the purposes of them is to shed light on the relationship between local luminance and local contrast in order to estimate the image quality for different appearing images. However, their method is not clear whether there is an ideal dependence between dispersion and location for good visual quality images.

In their [1] method for example, takes the local standard deviation and the local average as estimators and assumes that the local standard deviation should be proportional to the pixel average (a situation analogous to that in Weber's law) for certain types of images. This in fact is not true in general since, as mentioned, many good quality images have a correlation coefficient of local dispersion and location very near to zero. With a slightly different definition of contrast, it is argued in [20] that there are independence between luminance and contrast in natural scenes.

Restrepo and Ramponi [21] considered that scatter plots of local dispersion versus location (d-l plots, for short) carry a fair amount of the information in the image. And then they proposed a word descriptor which classifies the points as belonging to one of four main regions, counting them, normalizing and ordering the numbers.

The four regions in their result are labeled as A, B, C and D and correspond to high-contrast/medium-luminance, low-contrast/low-luminance, medium-contrast/medium-luminance and low-contrast/high-luminance., respectively, and these are illustrated as in Fig. 2.9.

To obtain a word descriptor, however, this method requires very high computational complexity, because they have to compute the pixel intensity histogram and executing of dispersion and location distribution. It is very difficult or may be impossible to commercialize since these computing operations are mathematically complex, and those need the powerful and high performance system, as well.

In this chapter, we introduce a novel normalized numerical image descriptor and suggest the validity of the proposed algorithm by comparing with the word descriptor [21]. This can estimate the image quality more clearly and objectively

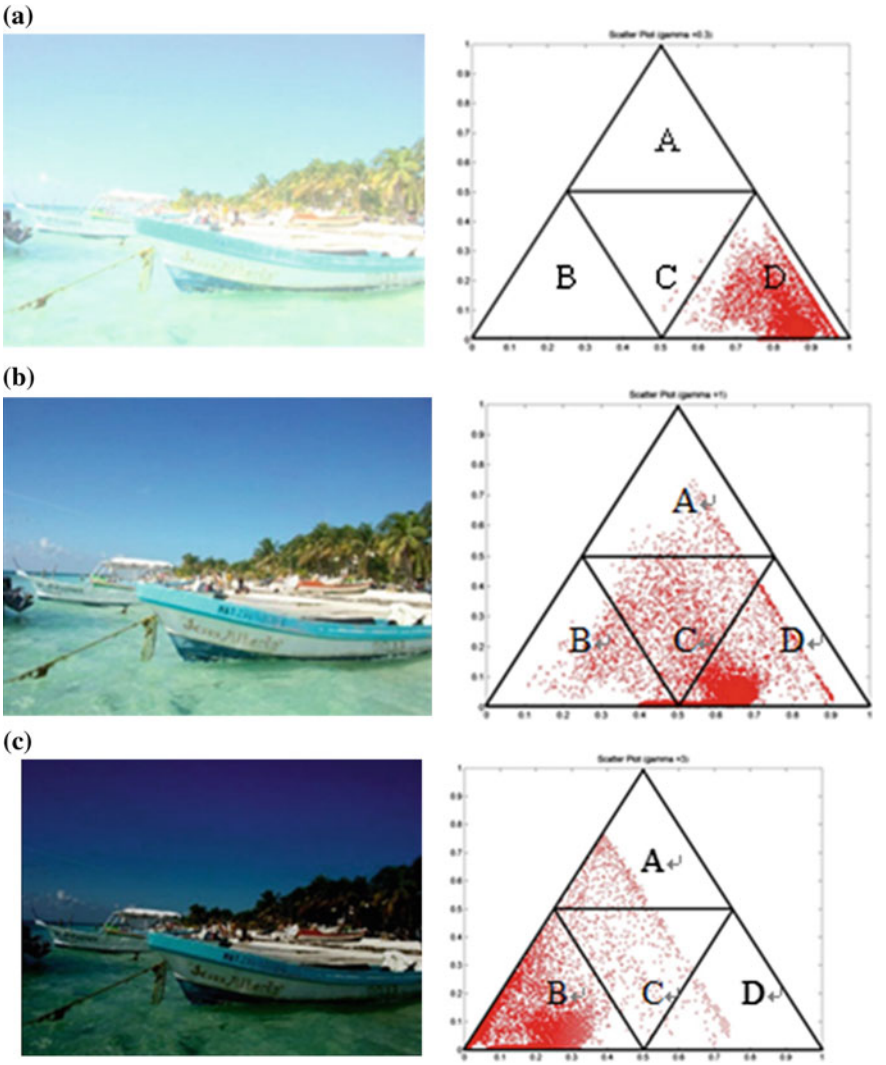

Fig. 2.9 Three "boat" images with different gamma values and their scattering chart. **a** $\gamma = 0.5$, **b** $\gamma = 1$, **c** $\gamma = 1.5$

than previous works. The image luminance assessment descriptor is based on the histogram calculation; we use the pixel data as weighted value. Also for the image contrast assessment descriptor, we use the same concept of luminance assessment. These two operations consist of just summation and multiplication. To verify our algorithm, we compare between the results of proposed and the results of the word descriptor by using several images with different gamma value as from 0.1 to 3.

Numerous gamma correction algorithms are based on the histogram. Its basic concept is that image quality can be enhanced using a kind of histogram equalization, it can be expressed as

$$s = T(r) \tag{2.15}$$

where s is the gamma corrected image by using transfer function T( ), r is the data of original image. Thus, gamma correction is finding the suitable transfer function T( ). The histogram of a digital image with gray level in the range $[0, L-1]$ is a discrete function $h(r_k) = n_k$, where r_k is the k-th gray level and n_k is the number of pixels in the image having gray level r_k. The numerical luminance descriptor (*LD*) can be expressed as

$$LD = \sum_{k=0}^{L-1} r_k n_k \tag{2.16}$$

And we apply normalization into Eq. (2.16), then

$$NLD = \frac{1}{LN} \sum_{k=0}^{L-1} r_k n_k, \quad 0 \leq NLD \leq 1 \tag{2.17}$$

where L is maximum quantized value and N is image size, they are taken from the original image. In Eq. (2.17), we understand that if an image has a normalized luminance descriptor (*NLD*) value becomes 1 and this image is estimated as bright image. On the other hand, if it is near to 0 then this image expressed as dark. From these result, our algorithm suggests that the objective luminance assessment degree with numeric representation. We present example images of "boat" with different gamma value and each scattering chart are shown in Fig. 2.10. As shown in Table 2.1, our proposed algorithm has same result by simple method as compared with the word descriptor method.

However, this normalized luminance descriptor (*NLD*) does not include the contrast information. Thus we have to consider the contrast estimation method. The contrast information can be estimated using the distribution of the difference between maximum and minimum pixel value of the image, thus it can be expressed as $c = r_{\max} - r_{\min}$.

As same with the luminance descriptor, the histogram of a contrast distribution with gray level in the range $[0, L-1]$ is a discrete function $h(c_l) = b_l$, where cl is the l-th block contrast value and b_l is the number of blocks in the image having contrast value c_l. Here, $c_l = b(r_{\max} - r_{\min})_l$ and $b(r_{\max} - r_{\min})_l$ is the contrast value in l-th block. Thus, the numerical contrast descriptor (CD) can be expressed as

$$CD = \sum_{l=0}^{B-1} c_i b_i \tag{2.18}$$

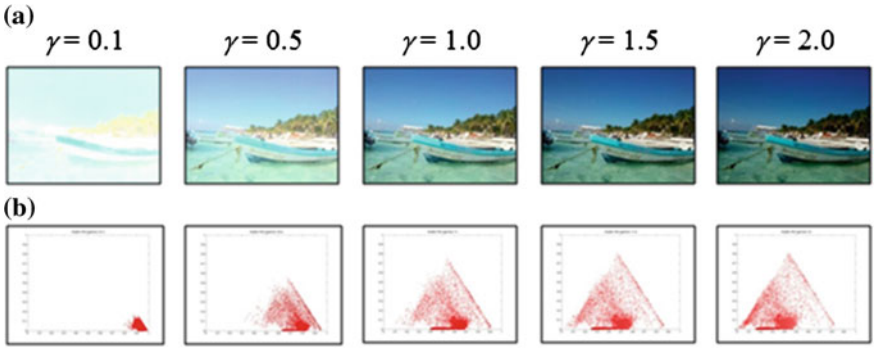

Fig. 2.10 Example images of "boat" with different gamma value and each scattering chart. **a** Images with difference gamma value: image resolution = 640 × 480, **b** scattering charts for each gamma value

Table 2.1 NLD for each gamma value and block size

Gamma Block size	0.1	0.5	1	1.5	2
global	0.94	0.74	0.56	0.42	0.33
4 × 4	0.94	0.74	0.56	0.42	0.33
8 × 8	0.94	0.74	0.56	0.43	0.33
16 × 16	0.94	0.74	0.56	0.43	0.33

And we apply normalization into Eq. (2.18), then

$$NCD = \frac{1}{LB}\sum_{l=0}^{B-1} c_i b_i, \quad 0 \le NCD \le 1 \tag{2.19}$$

where B is the total number of segmented block in the image. In Eq. (2.19), we understand that if an image has a normalized contrast descriptor (NCD) value near to 1 then this image is estimated as high contrast image, whereas if it is near to 0 then this image is low contrast. From these result, it also suggests the objective contrast. Therefore, the image quality assessment can be represented as Eq. (2.20) by combining with Eqs. (2.16) and (2.18).

$$NIQ = (NLD, NCD) \tag{2.20}$$

And its results for Fig. 2.10 are shown in Table 2.2.

In another example image, "gravelly field," as shown in Fig. 2.11 is one such representative image of the relatively high contrast. The NCD assessment in this chapter can clearly and objectively express the image quality which has same meaning compared with the scattering method or word descriptor.

Table 2.2 *NIQ* = (*NLD*, *NCD*) for each gamma value and block size of "boat" image

Gamma Block size	0.1	0.5	1	1.5	2
4 × 4	(0.94, 0.02)	(0.74, 0.06)	(0.56, 0.08)	(0.42, 0.09)	(0.33, 0.10)
8 × 8	(0.94, 0.03)	(0.74, 0.10)	(0.56, 0.17)	(0.42, 0.15)	(0.33, 0.15)
16 × 16	(0.94, 0.04)	(0.74, 0.15)	(0.56, 0.21)	(0.42, 0.22)	(0.33, 0.22)

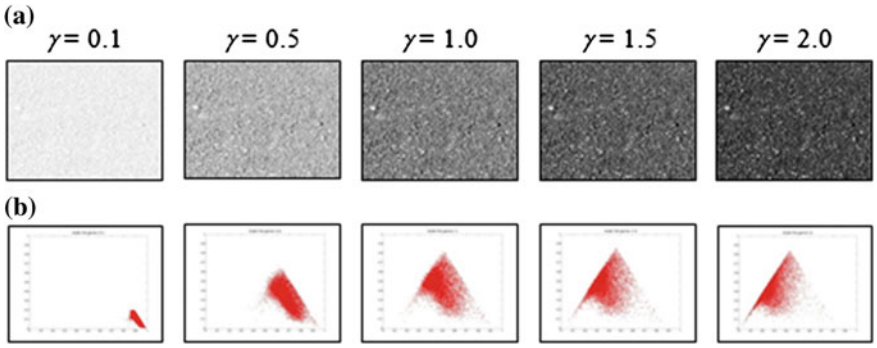

Fig. 2.11 Example images of "gravelly field" with different gamma value and each scattering chart. **a** Images with difference gamma value: image resolution = 640 × 480, **b** scattering charts for each gamma value

Table 2.3 *NIQ* = (*NLD*, *NCD*) for each gamma value and block size of "gravelly field" image

Gamma Block size	0.1	0.5	1	1.5	2
4 × 4	(0.93, 0.09)	(0.70, 0.30)	(0.51, 0.39)	(0.37, 0.40)	(0.28, 0.37)
8 × 8	(0.93, 0.14)	(0.70, 0.46)	(0.51, 0.58)	(0.37, 0.59)	(0.28, 0.55)
16 × 16	(0.93, 0.16)	(0.70, 0.57)	(0.50, 0.71)	(0.37, 0.72)	(0.28, 0.69)

As shown in Tables 2.1, 2.2 and 2.3, the *NLD* maintains almost same values without concern of block size, but the *NCD* has different values according to the images. Generally, the segmented block size is decided by using Shannon's ratio-distortion (*RD*) cost. But the study for this area is mainly studied in mode decision site since it is as another research area. Therefore, we only use widely used the 16 × 16 block segmentation in this chapter.

2.2.1.2 Experiments for Normalized Numerical Image Descriptor

We played the comparison experiment with word descriptor (or scattering chart) method to verify proposed algorithm. For the word descriptor, we followed [19], and for proposed algorithm process as below;

Table 2.4 $NIQ = (NLD, NCD)$ for each gamma value and block size of "airplane" image

Gamma Block size	0.1	0.5	1	1.5	2	2.5	3
4 × 4	(0.96, 0.03)	(0.81, 0.10)	(0.67, 0.14)	(0.56, 0.16)	(0.47, 0.16)	(0.40, 0.16)	(0.34, 0.15)
8 × 8	(0.96, 0.04)	(0.82, 0.16)	(0.68, 0.23)	(0.57, 0.26)	(0.48, 0.27)	(0.41, 0.26)	(0.35, 0.25)
16 × 16	(0.96, 0.06)	(0.82, 0.22)	(0.68, 0.32)	(0.57, 0.36)	(0.48, 0.37)	(0.41, 0.36)	(0.35, 0.34)

Step 1: set a segmented block size from among these; global, 4 × 4, 8 × 8, and 16 × 16.
Step 2: calculation for the normalized numerical luminance descriptor

(1) Choose one pixel data from each block
(2) Normalize the chosen pixel data
(3) Obtain the summation of these normalized pixel data
(4) Obtain the normalized numerical luminance descriptor by dividing the number of block.

Step 3: calculation for the normalized numerical luminance descriptor

(1) Find the maximum and the minimum pixel data in each block
(2) Normalize the difference in both of them which is obtained at 1)
(3) Perform the summation of these normalized differences
(4) Obtain the normalized numerical contrast descriptor by dividing the number of block.

In this chapter, we present total four experiments' results wise "Airplane", "Baboon", Butterfly", and "Uniform noise" sample images. The resolution sizes of them are 200 × 200, 200 × 200, 500 × 500, 356 × 356, respectively, and these are 24-bit RGB bitmap color images. To estimate image quality of them, we convert color image to gray level image by using as

$$Y = 0.3R + 0.6G + 0.1B \tag{2.21}$$

The experiments' results are as below.

This chapter has described the normalized numeric image quality descriptor. It suggests the clear and objective image quality assessment degree. The word descriptor requires the high computational complexity, whereas this proposed method is simple and easily obtained using the summation and mean value. To perform the gamma correction algorithm to enhance the image quality, the assessment of image quality must be executed first since we can find image quality enhancement method depending upon what image quality is. In numerous gamma correction algorithms, most computations belong to this image quality estimation (Tables 2.4, 2.5 and 2.6).

Therefore, clear and objective image descriptor by this chapter can increase the efficiency and performance of numerous gamma correction or wide dynamic range algorithms.

Table 2.5 $NIQ = (NLD, NCD)$ for each gamma value and block size of "baboon" image

Gamma Block size	0.1	0.5	1	1.5	2	2.5	3
4 × 4	(0.93, 0.04)	(0.70, 0.14)	(0.50, 0.19)	(0.36, 0.19)	(0.28, 0.18)	(0.20, 0.16)	(0.15, 0.14)
8 × 8	(0.93, 0.06)	(0.70, 0.21)	(0.50, 0.28)	(0.36, 0.29)	(0.28, 0.27)	(0.19, 0.23)	(0.14, 0.21)
16 × 16	(0.93, 0.08)	(0.70, 0.29)	(0.50, 0.38)	(0.36, 0.39	(0.28, 0.37)	(0.20, 0.33)	(0.15, 0.29)

Table 2.6 $NIQ = (NLD, NCD)$ for each gamma value and block size of "butterfly" image

Gamma Block size	0.1	0.5	1	1.5	2	2.5	3
4 × 4	(0.91, 0.04)	(0.62, 0.12)	(0.41, 0.14)	(0.28, 0.13)	(0.19, 0.12)	(0.15, 0.11)	(0.11, 0.08)
8 × 8	(0.91, 0.07)	(0.62, 0.22)	(0.41, 0.26)	(0.28, 0.25)	(0.19, 0.23)	(0.15, 0.20)	(0.11, 0.18)
16 × 16	(0.90, 0.10)	(0.62, 0.32)	(0.41, 0.40)	(0.28, 0.39	(0.19, 0.36)	(0.15, 0.32)	(0.11, 0.29)

2.2.2 Gamma Correction Based on Tone Mapping Method

2.2.2.1 Introduction

In everyday life we experience real world scene displays the wide range of luminance values. The range of light we experience in the course of day is vast. The light of the noon sun can be as much as 10 million times more intense than moonlight. The human visual system is capable of perceiving scenes spanning five orders of magnitude, and adapting more gradually to over nine orders of magnitude. Although adaptation provides visual functioning over a wide range of ambient intensities, this does not mean that we see equally well at all intensity levels. For dim light our eyes are very sensitive to luminance and we can detect small difference in illumination, but acuity and colour sensitivity reduces. That is why we can't read in twilight. In day light we have sharp colour vision but absolute sensitivity is low and to detect luminance difference it should be great enough (Figs. 2.12, 2.13 and 2.14).

In practice media used to display these images is either a video display or a print on chapter and they cannot reproduce the computed luminance, or span more than a few orders of magnitude. The realistic image synthesis has shown that, it is possible to produce images that convey the appearance of the simulated scene by mapping to a set of luminance that can be produced by the display media.

It is widely agreed that image reproduction algorithms should aim to preserve intensity ratios. Using system dynamic range as a measure, we can determine in advance whether preserving intensity ratios is possible or not. If the original scene has a dynamic range that is less than or equal to the system dynamic range, we can preserve intensity ratios. Rendering the image in this scenario is a simple process. However if the original scene's dynamic range is greater than the system dynamic range, intensity ratios cannot be preserved and dynamic range compression algorithms are needed.

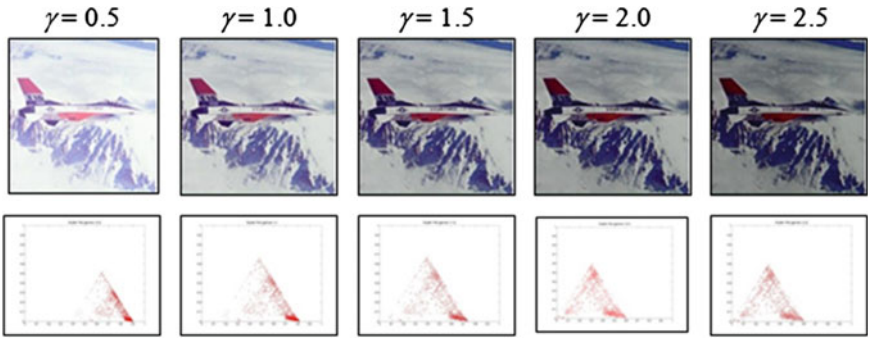

Fig. 2.12 Test images of "airplane" with different gamma value and each scattering chart

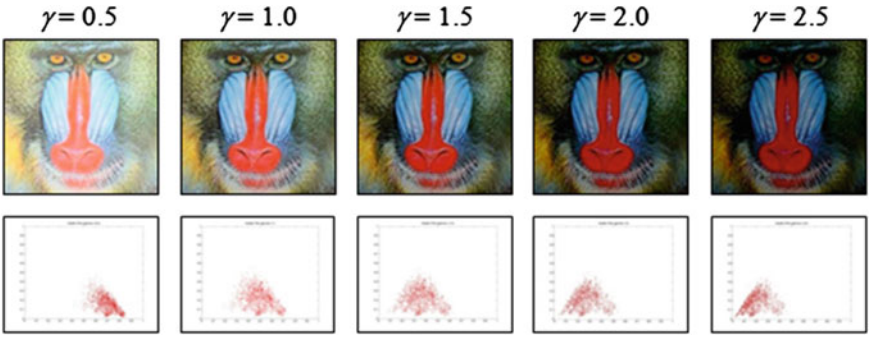

Fig. 2.13 Test images of "baboon" with different gamma value and each scattering chart

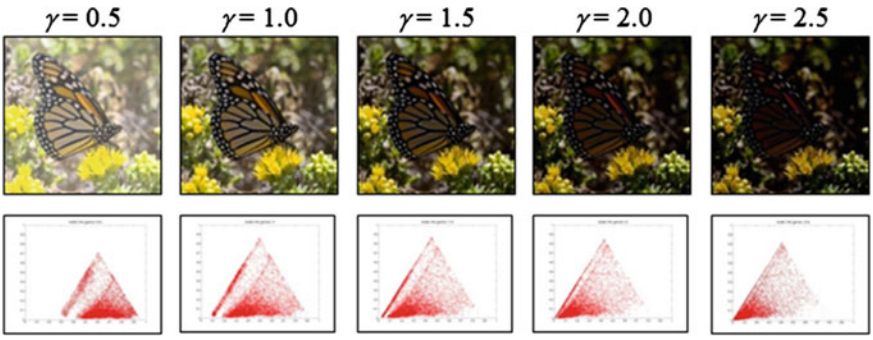

Fig. 2.14 Test images of "butterfly" with different gamma value and each scattering chart

In a typical scene that poses problem for tone reproduction both for photography and computer graphics image synthesis system—an outside sunlit landscape looked through the window. Human eyes can easily adapt the luminance level.

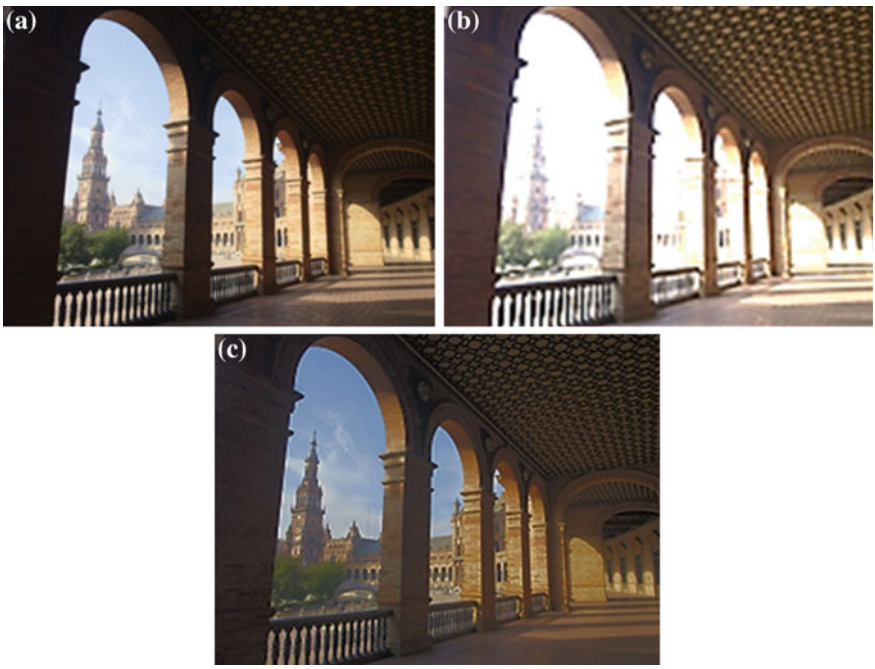

Fig. 2.15 Example images for high dynamic range: **a** underexposed photograph, **b** over exposed photograph, **c** high dynamic range image

But for photo, this is either overexposed or the dark region is under exposed. This shown in Fig. 2.15a, b along with corrected image Fig. 2.15c with proposed new method.

In this chapter, we will be using this computationally efficient and intuitive method and this approach addresses over or under exposure problem associated with the images capturing wide range of luminance. This tone reproducing operator or tone mapping operator is built from image own data and reliably map high dynamic luminance to display luminance.

2.2.2.2 Survey of Other Approaches and Research Trends

Jeffrey et al. [22] have grouped High Dynamic range image algorithms into two categories: tone reproduction curves (TRCs) and tone reproduction operators (TROs). TRCs operate point-wise on the image data and comparatively simpler. Author has reviewed several high dynamic range algorithms based on visual sensitivity. These are the visual concepts we have utilized while designing this method.

TRO use the spatial structure of the image data and attempt to preserve local image contrast by maintaining the local intensity ratios. TRO's detail preserving local gain control algorithms are developed by Pattnaik and Yee [23]. Ramponi [24] have proposed one such special transformation method based on Retinex theory. The comprehensive details can be found in [24–26]. These methods produce satisfactory results. But these are computationally heavy and memory consuming. Jian Duan and Bressan [27] have used Histogram adjustment based local tone mapping method. Segmentation of image and adaptive contrast adjustment has produced good results.

Pattanaik and Ferwada [28] have developed a computational model of visual adaptation for realistic image synthesis based on psychophysical experiments that accounts for changes in special acuity and color sensitivities as a function of light level. This may be good guideline for any method.

A tone mapping operator has been proposed by Tumblin and Rushmier [29] using the brightness function based on Steven and Steven [30]. Here preservation of the brightness is at the expense of visibility. TRC operate point-wise on the image data, making the algorithms simple and efficient. Popularly used TRC functions are Power or Logarithmic mapping. These functions compress the dynamic range. A visibility matching tone reproduction operator based on logarithmic function is proposed by Larson and Rushmeier [31]. They have accounted for glare, special acuity and colour sensitivities. It requires additional histogram adjustment methods to reduce its contrast exaggeration.

Our work is greatly inspired by these chapters. After studying various methods, this new method is designed to keep simple computation and utilises successful element of past methods and adds new element to make it efficient. Our chapter utilise TRC based tone operator which is computationally simple yet gives better results.

2.2.2.3 Main Features of Proposed Method

Visibility maintained along with brightness and contrast. Hence the fine details of the images can be seen clearly without histogram adjustments. For getting required amount of contrast in the image, compression factor is used with tan function. The method essentially increases the contrast in the image. But exaggerated contrast disturbs the correct visual impact and hence we need the adjustment which will be done by minimizing the gap between the luminance counts.

The main features of proposed method are

(1) Simple and intuitive step solution which gives better contrast for brighter region of image and visibility for dark region.
(2) Dark images are corrected as well.
(3) Dynamic range compression using adjustable variable factor.
(4) It uses sophisticated adoption factor based on trigonometric function Tan and root power to achieve the brightness and contrast level.

(5) No Histogram adjustments needed.
(6) Works in both for fully automaized calculation as well as user control.

For this new method approach we will work on luminance of image and start with the Histogram. For high dynamic range luminance the above example of outdoor sunlight and the inside corridor of the structure or the following case of dark indoor on brightly lit outdoor landscape, the histogram shows that luminance level is occurred in clusters rather than uniform distribution over the range.

It is studied that any method fails that uses a single adaptation level that maps a large range of the sparsely populated real world luminance levels to large range of display level. As described above eyes are sensitive to the bright region with respect to dark region. To sense the difference in the bright light it should be big enough. But in dim light this small difference of illumination is easily detectable.

Step 1: We will start with undistorted image and its histogram.
The histogram of digital image with L the total possible intensity levels in the range is defined as discreet function

$$h(k) = n_k \tag{2.22}$$

where $h(k)$ is k-th intensity level and n_k is number of pixels at intensity k. Cumulative Probability frequency distribution $P(k)$ is given by

$$P(k) = \sum_{k_n < k} T(k_n)/T \tag{2.23}$$

where T is total number of samples (Fig. 2.16).
Step 2: Let Min and Max represent the level of minimum and maximum intensity present in the image.
Step 3: The result will look like as following probability distribution function in Fig. 2.17.
The new probability frequency distribution $P_k(K)$ can be calculated and plotted with respect to Minimum and Maximum level of intensity present in the image and the cumulative distribution will look like Fig. 2.18.
Step 4: We will be following tone reproduction operator for calculating display range as

$$\mathrm{Exp}(DR) = C_f\left\{\sqrt{[n]}\tan(p_k(k) \times 1.5)\right\} + \log(LD_{\min}) \tag{2.24}$$

where DR is the display range luminance value, C_f notes a compression factor, $L_{\min}$ is the display minimum luminance level in the image.
The display range is restricted less than the difference value k_1 (i.e. $k_1 = \mathrm{Max} - \mathrm{Min}$). Various result shows that parameter compact will vary in the range of 0.1–5.54. As this will be maximum limits of natural log limits value 255. But the world luminance to display is as shown Fig. 2.19.

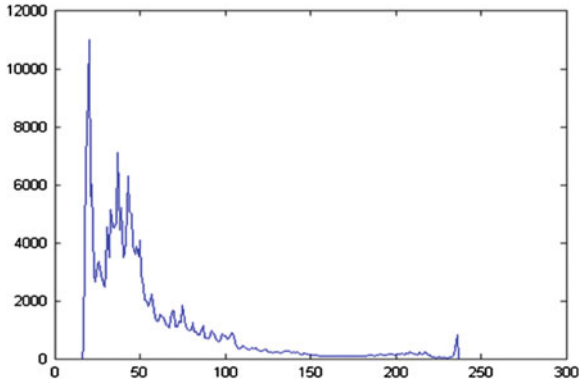

Fig. 2.16 House on brightly lit landscape (size of image: 600 × 400)

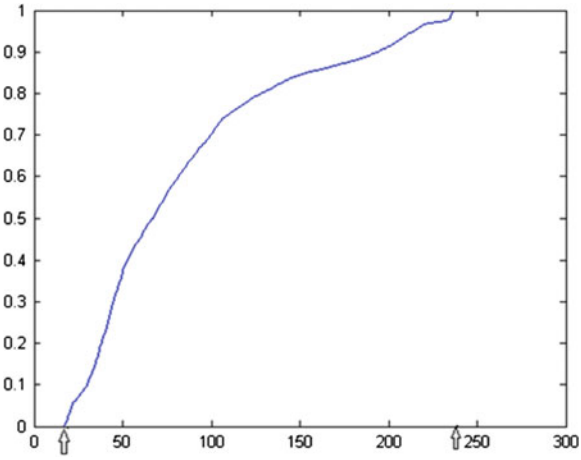

Fig. 2.17 *Curve* showing probability distribution function

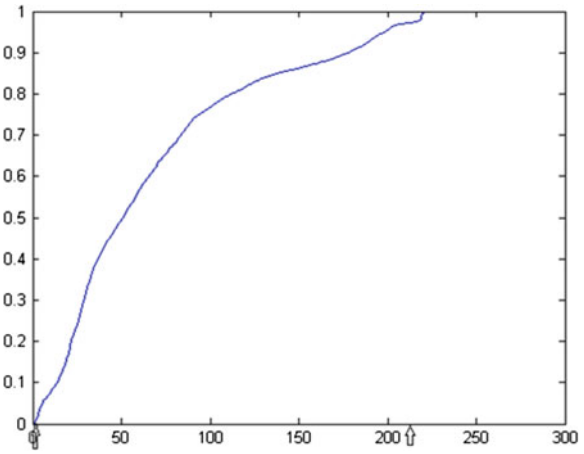

Fig. 2.18 Probability distribution replotted with respect to minimum and maximum luminance

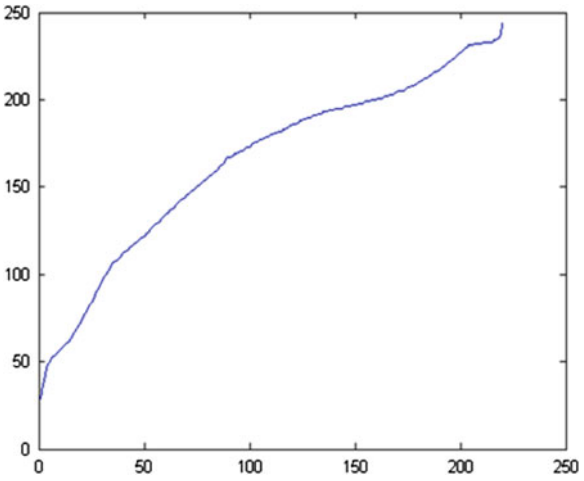

Fig. 2.19 The world luminance to display luminance

This can be done by following loop code.

For c C_f 0.1 to 5 in steps 0.1

For each k level

if $k < LD_{max} - LD_{min}$

$$\text{Exp}(DR) = C_f\left\{\sqrt[n]{tan(p_k(k) \times 1.5)}\right\} + log(LD_{min})$$

else

$$\text{Exp}(DR) = C_f\left\{\sqrt[n]{tan2(p_k(k) \times 1.5)}\right\} + log(LD_{min})$$

endif

Break if range exceeds the k1

Then range as defined above

End for

End for

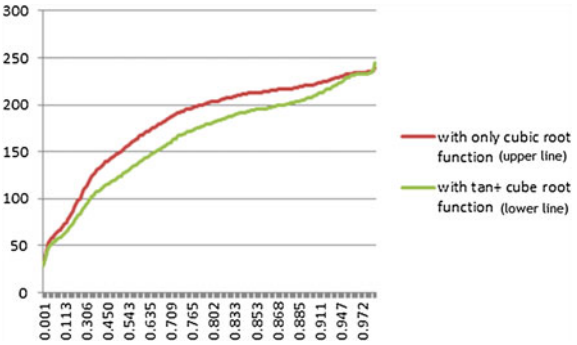

Fig. 2.20 Effect comparison of with tan and only cube root function

Figure 2.20 shows effect of trigonometric function tan with cube-root function and using only cube root function. Using tan it does add the required contrast in the image. The tan functionality curve is shown in figure and to utilize its full positive range the multiplication factor of 1.5 is used.

Contrast of the image is defined as the ratio of the difference in foreground and background to the background and therefore, adding value to both actually reduces the contrast. Merely using the root function gives benefit of better visibility but it is at the cost of losing fine detail especially in bright region. Hence we have added tan functionality. This one acts as complimentary to cube-root function. So we have taken the advantage of better visibility by using power root function and to overcome its disadvantage tan function is used along-with it.

Note that tan curve at higher luminance level is steep which gives better contrast. The image range get compressed aggressively at sparsely populated region compared to densely populated region and yields the desirable range using the adjustment of compression factor along with contrast adjusting tan function. Sometimes method results into enhanced amount of contrast in the image.

The exaggerated amount of contrast is reduced by closing the gap between two consecutive intensity bin and should be kept as minimum as possible maintaining the intensity ratio. For this the gap between the two levels is calculated and will be reduced linearly (Fig. 2.21).

Step 5: At last using this mapping function, display is reproduced by subtracting minimum luminance value of the image (min).

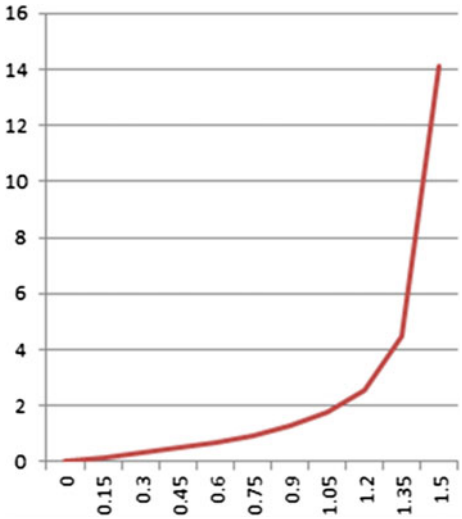

Fig. 2.21 Tan function

Fig. 2.22 The corrected image with proposed method (sample 1) **a** original image, **b** corrected image

2.2.2.4 Test Examples

See Figs. 2.22, 2.23, 2.24, 2.25, 2.26, 2.27 and 2.28.

2.2.2.5 Comparison with Others

In this chapter we have presented a novel method based on the compression for high dynamic range images. After studying various method this new method is developed to keep fast, computationally simple and automatized. It can have user control for desired control on brightness or contrast. It enhances the contrast of the

Fig. 2.23 The corrected image with proposed method (sample 2) **a** original image, **b** corrected image

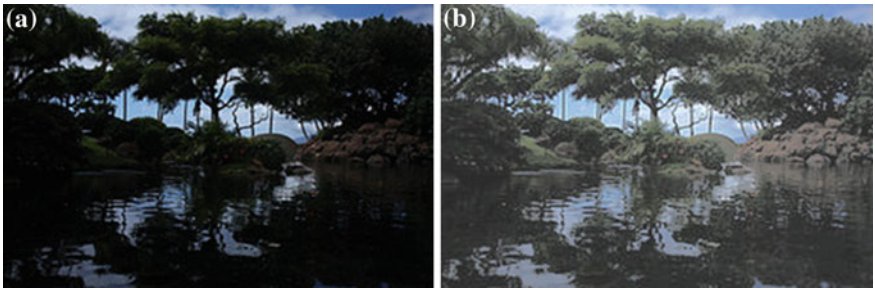

Fig. 2.24 The corrected image with proposed method (sample 3) **a** original image, **b** corrected image

Fig. 2.25 The corrected image with proposed method (sample 4) **a** original image, **b** corrected image

bright region of the image and at the same time increases the visibility of the dark region. For perfect contrast achievement the range variable compression factor is used along-with trigonometric tan function. Also, this is the automated calculation which yield the better result as shown in the examples.

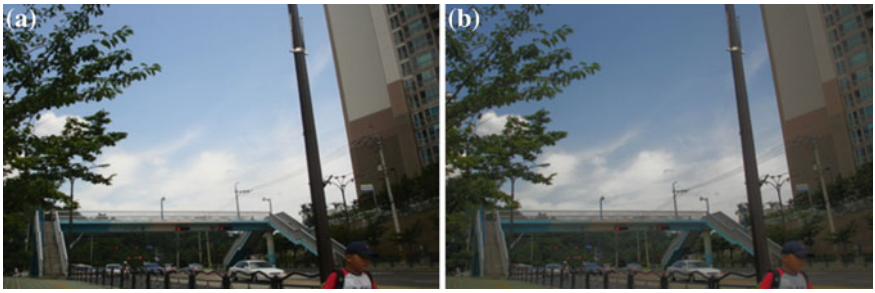

Fig. 2.26 The corrected image with proposed method (sample 5) **a** original image, **b** corrected image

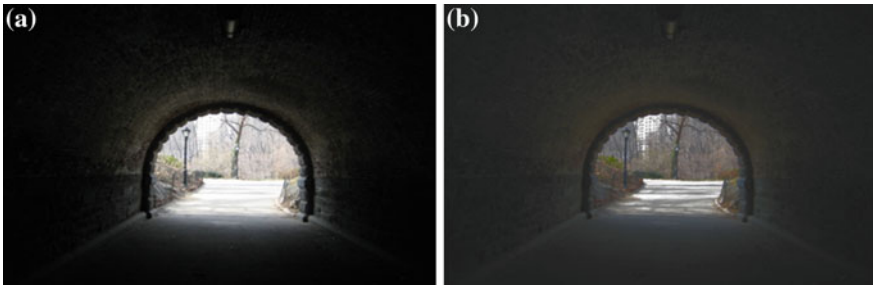

Fig. 2.27 The corrected image with proposed method (sample 6) **a** original image, **b** corrected image

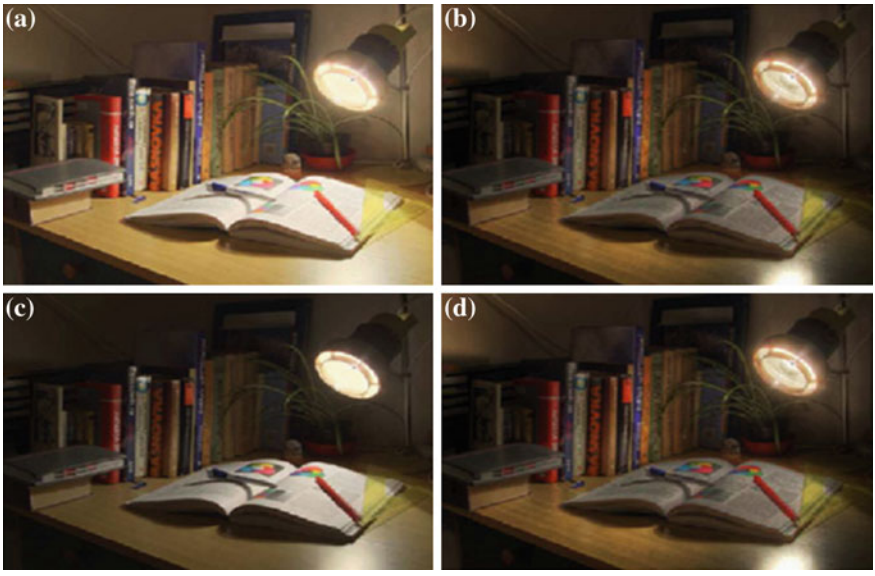

Fig. 2.28 Comparison with other algorithms **a** Pattanaik (02), **b** Durand (02), **c** Tumblin (99), **d** proposed

References

1. D.C. Brown, Decentering distortion of lenses. Photogram Eng. Remote Sens. **24**, 555–566 (1966)
2. D.C. Brown, Close-range camera calibration. Photogram. Eng. Remote Sens. **42**, 855–866 (1971)
3. J. Heikkila, O. Silven, in *Proceedings of the 13th International Conference on "Calibration procedure for short focal length off-the-shelf CCD cameras," in Pattern Recognition*, vol. 1 (1996), pp. 166–170
4. M. Yan, Z. Hanqi, What you see is what you get [self-calibrating camera lens distortion]. IEEE Robot. Autom. Mag. **11**, 123–127 (2004)
5. M. Ahmed, A. Farag, Nonmetric calibration of camera lens distortion: differential methods and robust estimation. IEEE Trans. Image Process. **14**, 1215–1230 (2005)
6. F. Devernay, O. Faugeras, Straight lines have to be straight. Mach. Vis. Appl. **13**, 14–24 (2001)
7. B. Prescott, G.F. McLean, Line-based correction of radial lens distortion. Graph. Models Image Process. **59**, 39–47 (1997)
8. H. Farid, A.C. Popescu, Blind removal of lens distortion. J. Opt. Soc. Am. A **18**, 2072–2078 (2001)
9. J.A. Nelder, R. Mead, A simplex method for function minimization. Comput. J. **7**(4), 308–313 (1965)
10. M.T. Ahmed, A.A. Farag, in *Proceedings of the 2001 IEEE Computer Society Conference on "Differential Methods for Nonmetric Calibration of Camera Lens Distortion," in Computer Vision and Pattern Recognition CVPR 2001*, vol. 2 (2001), pp. II-477–II-482
11. R. Cucchiara et al., in *Proceedings of 12th International Conference on "A Hough Transform-Based Method for Radial Lens Distortion Correction," in Image Analysis and Processing* (2003), pp. 182–187
12. S. Graf, T. Hanning, in *IEEE Computer Society Conference on "Analytically solving radial distortion parameters," in Computer Vision and Pattern Recognition, CVPR 2005*, vol. 2 (2005), pp. 1104–1109
13. K. Sirisantisamrid et al., in *IEEE Region 10 Conference "A Simple Technique to Determine Calibration Parameters for Coplanar Camera Calibration," in TENCON 2004*, vol. 1 (2004), pp. 677–680
14. R. Sagawa et al., in *IEEE/RSJ International Conference on "Calibration of Lens Distortion by Structured-Light Scanning," in Intelligent Robots and Systems (IROS 2005)*, (2005), pp. 832–837
15. W. Yu, Image-based lens geometric distortion correction using minimization of average bicoherence index. Pattern Recogn. **37**, 1175–1187 (2004)
16. T. Nave, J.M. Francos, in *2nd International Conference on "Global Featureless Estimation of Radial Distortions," in Signal Processing and Communication Systems, ICSPCS 2008* (2008), pp. 1–11
17. R. Tsai, A versatile camera calibration technique for high-accuracy 3D machine vision metrology using off-the-shelf TV cameras and lenses. IEEE J. Robot. Autom. **3**, 323–344 (1987)
18. Z. Wentao et al., A high-precision camera operation parameter measurement system and its application to image motion inferring. IEEE Trans. Broadcast. **47**, 46–55 (2001)
19. J.P. Oakley, H. Bu, Correction of simple contrast loss in color images. IEEE Trans. Image Process. **16**(2), 511–522 (2007)
20. V. Mante, R.A. Frazor, V. Bonin, W. Geisler, M. Carandini, Independence of luminance and contrast in natural scenes and in the early visual system. Nat. Neurosci. **8**(12), 1690–1697 (2005)

21. A. Restrepo (Palacios), G. Ramponi, Word descriptors of image quality based on local dispersion-versus-location distributions, in *16th EUSIPCO 2008*, Lausanne, Switzerland, 25–29 August 2008
22. G. Ramponi, Adaptive contrast improvement for still images and video frames, in *IEEE—EURASIP Workshop on Nonlinear Signal and Image Processing, NSIP-07*, Bucharest, Romania, 10–12 Sept 2007
23. S.N. Patnaik, H. Yee, Adaptve gain contol for high dynamic range image display, in *Proceedings of Spring Conference in Computer Graphics (SCCG2002)*, Budmerice, Slovak Republic, 24–27 April 2002
24. G. Guarnieri, S. Marsi, G. Ramponi, High dynamic range image display with halo and clipping prevention. IEEE Trans. Image Process. **20**(5), 1351–1362 (2011)
25. K. Chiu, M. Herf, P. Shirley, S. Swamy, C. Wang, K. Zim-merman, Spatially nonuniform scaling functions for high contrast images, in *Proceedings of Graphics Interface '93,* Toronto, Canada, May 1993, pp. 245–253
26. R. Fallal, D. Lischinski, M. Werman, Gradient domain high dynamic range compression, in *Proceedings of SIGGRAH* (2002)
27. J. Duan, M. Bressan, C. Dance, G. Qiu, Tone-mapping high dynamic range images by novel histogram adjustment. Pattern Recogn. **43**(5), 1847–1862 (2010)
28. J.A. Ferwerda, S.N. Pattanaik, P. Shirley, D.P. Greenberg. A model of visual adaptation for realistic image synthesis. in *Proceedings of the SIGGRAPH'96* (1996), pp. 249–258
29. J. Tumblin, H. Rushmeier, Tone reproduction for realistic images. IEEE Comput. Graphics Appl. **13**, 42–48 (1993)
30. S.S. Stevens, J.C. Stevens, Brightness function: parametric effects of adaptation and contrast. J. Optical Soc. Am. **53**, 1139 (1960)
31. G.W. Larson, H. Rushmeier, C. Piatko, A visibility matching tone reproduction operator for high dynamic range scenes. IEEE Trans. Visual. Comput. Graph. **3**, 291–306 (1997)

http://www.springer.com/978-94-017-9074-1

Algorithm & SoC Design for Automotive Vision Systems
For Smart Safe Driving System
Kim, J.; Shin, H. (Eds.)
2014, IX, 290 p. 247 illus., 2 illus. in color., Hardcover
ISBN: 978-94-017-9074-1